Jennions, S., Thomas, E., Schmidt, D., Lunt, D., & Ridgwell, A. (2015). Changes in benthic ecosystems and ocean circulation in the Southeast Atlantic across Eocene Thermal Maximum 2. *Paleoceanography*, *30*(8), 1059-1077. https://doi.org/10.1002/2015PA002821

AGU PUBLICATIONS

Paleoceanography

RESEARCH ARTICLE
10.1002/2015PA002821

Key Points:
- Benthic forams were most affected at the shallow Walvis Ridge site during ETM2
- Changing ocean circulation caused pronounced warming at intermediate depths
- Disruption of benthic ecosystems reduces bioturbation and affects drill core records

Supporting Information:
- Text S1, Tables S1–S4, and Figure S1
- Data Set S1

Correspondence to:
S. M. Jennions,
suzanne.jennions@bristol.ac.uk

Citation:
Jennions, S. M., E. Thomas, D. N. Schmidt, D. Lunt, and A. Ridgwell (2015), Changes in benthic ecosystems and ocean circulation in the Southeast Atlantic across Eocene Thermal Maximum 2, *Paleoceanography*, *30*, 1059–1077, doi:10.1002/2015PA002821.

Received 24 APR 2015
Accepted 7 JUL 2015
Accepted article online 14 JUL 2015
Published online 7 AUG 2015

Changes in benthic ecosystems and ocean circulation in the Southeast Atlantic across Eocene Thermal Maximum 2

S. M. Jennions[1], E. Thomas[2,3], D. N. Schmidt[1], D. Lunt[4], and A. Ridgwell[4,5]

[1]School of Earth Sciences, University of Bristol, Bristol, UK, [2]Department of Geology and Geophysics, Yale University, New Haven, Connecticut, USA, [3]Department of Earth and Environmental Sciences, Wesleyan University, Middletown, Connecticut, USA, [4]School of Geography, University of Bristol, Bristol, UK, [5]Department of Earth Sciences, University of California, Riverside, California, USA

Abstract Eocene Thermal Maximum 2 (ETM2) occurred ~1.8 Myr after the Paleocene-Eocene Thermal Maximum (PETM) and, like the PETM, was characterized by a negative carbon isotope excursion and warming. We combined benthic foraminiferal and sedimentological records for Southeast Atlantic Sites 1263 (1500 m paleodepth) and 1262 (3600 m paleodepth) to show that benthic foraminiferal diversity and accumulation rates declined more precipitously and severely at the shallower site during peak ETM2. As the sites are in close proximity, differences in surface productivity cannot have caused this differential effect. Instead, we infer that changes in ocean circulation across ETM2 may have produced more pronounced warming at intermediate depths (Site 1263). The effects of warming include increased metabolic rates, a decrease in effective food supply and increased deoxygenation, thus potentially explaining the more severe benthic impacts at Site 1263. In response, bioturbation may have decreased more at Site 1263 than at Site 1262, differentially affecting bulk carbonate records. We use a sediment-enabled Earth system model to test whether a reduction in bioturbation and/or the likely reduced carbonate saturation of more poorly ventilated waters can explain the more extreme excursion in bulk $\delta^{13}C$ and sharper transition in wt % $CaCO_3$ at Site 1263. We find that both enhanced acidification and reduced bioturbation during the ETM2 peak are needed to account for the observed features. Our combined ecological and modeling analysis illustrates the potential role of ocean circulation changes in amplifying local environmental changes and driving temporary, but drastic, loss of benthic biodiversity and abundance.

1. Introduction

Potential environmental impacts of increasing atmospheric CO_2 concentrations include warming, increased intensity of the hydrological cycle, and nutrient influx into the oceans, ocean stratification, ocean acidification, and increased hypoxia [*Caldeira and Wickett*, 2003; *Hutchins et al.*, 2007; *Solomon et al.*, 2009; *Coma et al.*, 2009; *Keeling et al.*, 2010; *Durack et al.*, 2012; *Pörtner et al.*, 2014], any or all of which may affect organisms and ecosystems. However, anticipating the biotic response to these multiple, potentially synergistic environmental parameters is challenging [*Bopp et al.*, 2013; *Melzner et al.*, 2013; *Norris et al.*, 2013; *Pörtner et al.*, 2014]. The response of species and ecosystems to changing environments has been, and continues to be, tested in mostly single-driver laboratory experiments, producing short-term, species-specific, and mainly physiological information [e.g., *Kroeker et al.*, 2010; *Pörtner et al.*, 2014]. Such experiments are valuable but reflect neither the complexity of the natural environment nor the adaptability of organisms on long time scales. Records of periods of past climate change, can, however, provide a detailed, quantifiable account of biotic response [e.g., *Hönisch et al.*, 2012; *Speijer et al.*, 2012]. A series of global warming and carbon release events ("hyperthermals") of variable intensity, occurring superimposed upon gradually rising global temperatures during the early to mid-Palaeogene [*Thomas and Zachos*, 2000; *Cramer et al.*, 2003; *Lourens et al.*, 2005; *Sluijs et al.*, 2007a], provide us with the potential for just such a test.

The best studied and largest of the hyperthermals is the Palaeocene-Eocene Thermal Maximum (PETM), with a variety of proxies indicating global warming due to emission of isotopically light carbon into the ocean-atmosphere [*Dunkley Jones et al.*, 2013]. In addition to warming, surface waters experienced rapid and sustained surface water ocean acidification [*Penman et al.*, 2014]. Oxygenation may have decreased globally during the PETM in response to warming, hydrological change, and carbon cycle feedback

[*Winguth et al*., 2012], with bottom water deoxygenation common along continental margins [*Thomas*, 1998; *Nicolo et al*., 2010] and the inferred occurrence of a broad expansion of oxygen minimum zones in the open ocean [*Zhou et al*., 2014]. Bottom water deoxygenation may have occurred at some open ocean southeast Atlantic sites [*Chun et al*., 2010; *Post et al*., 2015] but not in the Pacific [*Pälike et al*., 2014]. Nutrient availability and productivity may have increased in marginal basins but decreased in pelagic settings, although discussion is still ongoing due to regional difference in nutrient availability and productivity [*Gibbs et al*., 2006; *Thomas*, 2007; *Winguth et al*., 2012; *Schneider et al*., 2013; *Sluijs et al*., 2014; *Stassen et al*., 2015]. Knowledge of these changes is important because it allows exploration of the relationships between ecological sensitivity and environmental change.

In response to PETM environmental changes, phytoplankton and zooplankton expanded their ranges toward higher latitudes [*Kelly et al*., 1996; *Thomas and Shackleton*, 1996; *Crouch et al*., 2001; *Bralower*, 2002; *Hollis*, 2006; *Sluijs et al*., 2006; *Schneider et al*., 2013]. Species turnover, combined with evolution of short-lived "excursion taxa," resulted in transient changes in assemblage composition of marine pelagic groups [*Kelly et al*., 1996; *Gibbs et al*., 2006; *Raffi et al*., 2006; *Luciani et al*., 2007]. In addition, the PETM induced one of the largest recorded extinction events of deep-sea benthic foraminifera (35–40% species extinction) [*Thomas*, 1998, 2007; *Alegret et al*., 2010].

In contrast, much less is known about the marine biotic response to the smaller hyperthermals. We focus here on Eocene Thermal Maximum 2 (ETM2, previously described as H1), which occurred at ~53.7 Ma, i.e., about 1.8 Myr after the PETM [*Stap et al*., 2010a; *Westerhold et al*., 2012; *Littler et al*., 2014]. The ETM2 has been identified globally in marine and terrestrial records [*Lourens et al*., 2005; *Stein et al*., 2006; *Nicolo et al*., 2007; *Agnini et al*., 2009; *Stap et al*., 2009, 2010a, 2010b; *Sluijs et al*., 2009; *Clementz et al*., 2011; *Abels et al*., 2012; *d'Haenens et al*., 2012; *Dedert et al*., 2012; *Slotnick et al*., 2012]. The event is also well-documented in drill sites on Walvis Ridge (SE Atlantic Ocean) along a depth transect from ~3500 (Site 1262) to ~1500 m (Site 1263) paleodepth [*Zachos et al*., 2004a, 2004b]. The full duration of the ETM2 is estimated at ~100 kyr [*Stap et al*., 2009], with a carbon isotope excursion (CIE) magnitude of around −1.5‰, i.e., about half that of the PETM at the same site [*McCarren et al*., 2008]. The accompanying carbonate dissolution was also less severe [*Stap et al*., 2009], with a reduction by ~80% during the peak of the event ("ETM2 horizon," 40–55 ka after its onset) [*Lourens et al*., 2005; *Stap et al*., 2009] rather than complete dissolution of $CaCO_3$ as during the PETM [*Zachos et al*., 2005]. Peak warming was estimated at 3–4°C for bottom waters [*Stap et al*., 2010b], whereas estimates of surface water warming vary between ~2°C in the South Atlantic [*Lourens et al*., 2005; *Stap et al*., 2009, 2010a], ~2–2.5°C in the North Atlantic [*d'Haenens et al*., 2014], and ~4°C in Arctic [*Sluijs et al*., 2009], compared to 5–6°C averaged globally for the PETM [*Zachos et al*., 2005; *Sluijs et al*., 2007b; *Dunkley Jones et al*., 2013]. Unlike the PETM, there was no significant extinction of benthic foraminifers associated with ETM2, despite possible evolution of susceptible species in the 1.8 Myr between the events [*Lourens et al*., 2005; *Stap et al*., 2010a].

In this paper, we assess the biotic response of benthic ecosystems to ETM2 environmental changes at Walvis Ridge. We analyze a series of coupled climate and conceptual Earth system modeling experiments in order to explore the potential causes and consequences of benthic ecological change.

2. Materials and Methods

2.1. Samples

We obtained samples from two sites drilled during Ocean Drilling Program (ODP) Leg 208, Walvis Ridge, South Atlantic, Sites 1262 (palaeodepth 3600 m) and 1263 (palaeodepth 1500 m) [*Zachos et al*., 2004a, 2004b] (Figure 1). Cores from Holes 1262A and 1263C were sampled between 116.75–117.40 mcd and 294.27–295.53 mcd, respectively [*Lourens et al*., 2005; *Stap et al*., 2009], corresponding to topmost chron C24r, nannofossil zone P11, and planktic foraminiferal zone E4 (formerly P6) [*Zachos et al*., 2004a, 2004b]. The cores were sampled using a *u*-channel sampler, and the sediment sliced continuously at 0.5–1.0 cm resolution [*Stap et al*., 2009]. The carbonate content of these samples and bulk carbon and oxygen isotope values were reported by *Stap et al*. [2009].

We took a subset of samples for sediment analysis, at 1.0 cm resolution across ETM2 and 10–15 cm preevent and postevent, as defined by *Zachos et al*. [2004a, 2004b] (Tables S1 and S2 in the supporting information).

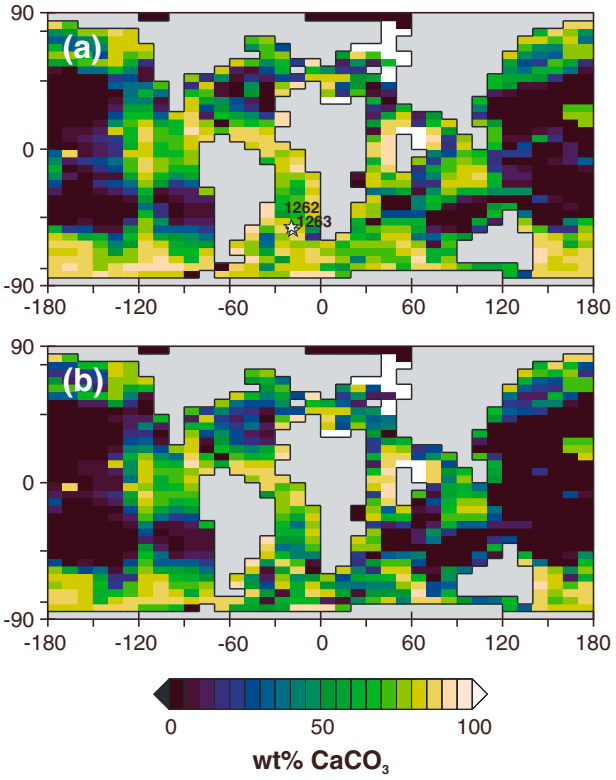

Figure 1. Illustration of the GENIE model grid for the late Paleocene/early Eocene configuration and showing the distribution of wt % $CaCO_3$ in surface sediments at the end of the model spin-up phase (a) with the location of Sites 1262 and 1263 marked by stars. (b) The pattern of wt % $CaCO_3$ corresponding approximately to peak ETM2 conditions.

Samples were washed through a 63 μm sieve using Reverse Osmosis deionized water, dried, and split into 63–150 μm and >150 μm size fractions. For benthic foraminiferal analysis a subset of the samples from *Stap et al.* [2009] was used, with a sample spacing of 2.0 cm across ETM2 and 10 cm above and below (Tables S3 and S4).

2.2. Age Model

In the ETM2 age model for Walvis Ridge, Stap and coworkers [*Stap et al.*, 2009] adjusted the terrigenous flux using Gaussian fitting techniques to optimally align the carbon isotope and calcium carbonate weight percent records. The result is an inferred fluctuating terrigenous flux at Site 1262 (higher during peak ETM2 conditions) and Site 1265 (lower during peak ETM2 conditions), with stable rates of terrigenous input at Sites 1263 and 1267. Disparity in the sign of terrigenous flux change across the event is somewhat unlikely, given the relative geographic proximity of the sites. Forcing an exact alignment of the primary features of the records is also potentially problematic because the apparent timing of events depends on bulk sediment rate and extent of bioturbation [*Ridgwell*, 2007], as well as differences in carbonate preservation [*Kirtland Turner and Ridgwell*, 2013], both of which can be expected to differ between sites and may vary in time.

We hence constructed an alternative age model, assuming a stable, site-specific terrigenous flux across the ETM2. There is evidence for generally elevated rates of chemical terrestrial weathering across the PETM [e.g., *Kelly et al.*, 2005; *Ravizza et al.*, 2001] and thus presumably also ETM2, but the total supply rate of particulate terrigenous material to Walvis Ridge may not necessarily have increased. In contrast, if the terrigenous input were dominated by airborne dust, a decrease under global warming would be expected [*Mahowald et al.*, 2006].

We calculated relative sediment age based on reported $CaCO_3$ wt % and dry bulk density [*Zachos et al.*, 2004a, 2004b] and using a terrigenous mass accumulation rate (TMAR) derived from an interval of sedimentation characterized by relatively stable climatic conditions immediately prior to ETM2 onset, and between precession cycle tie points of *Westerhold et al.* [2007], at 298.52–301.52 mcd at the shallow Site 1263 (~6 × 21 kyr cycles) and 118.5–121.83 mcd at the deep Site 1262 (~12 × 21 kyr cycles). The resulting TMARs were 0.154 g/cm^2/kyr for Site 1262 and 0.191 g/cm^2/kyr at Site 1263. In order to facilitate comparison with previous studies, we calculated terrigenous sedimentation rates for both sites: 0.13 cm/kyr at Site 1263 and 0.12 cm/kyr at Site 1262, and we adopt the zero relative age point defined by *Stap et al.* [2009]. Our age model is compared with that in *Stap et al.* [2009] in Figure 2. A full list of equations can be found in Text S1 in the supporting information.

2.3. Sedimentology and Benthic Foraminiferal Analysis

Site-specific bulk and carbonate mass accumulation rates (MARs) were calculated based on our age model. The $CaCO_3$ fine fraction (FF) (<63 μm) consists predominantly of calcareous nannofossils, the coarse fraction (CF) of planktic foraminifera. We hence used the coarse fraction MAR (>63 μm) to approximate the

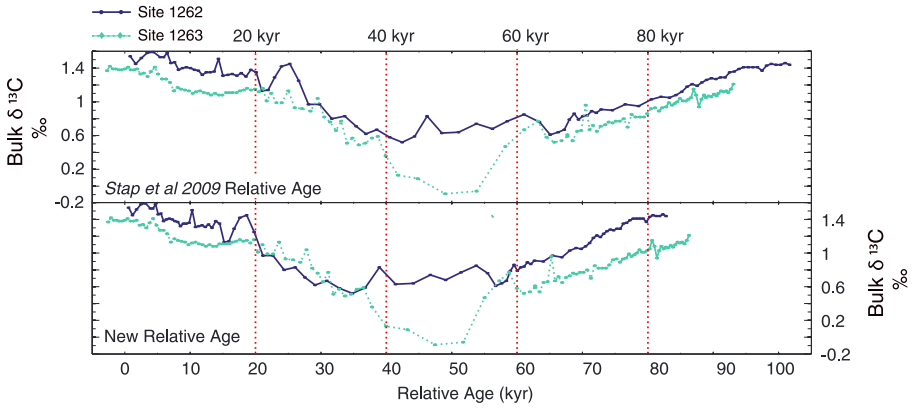

Figure 2. The bulk carbon isotope record from the shallow and deep sites (a) using the age model of *Stap et al.* [2009] and (b) using our age model.

foraminiferal mass accumulation rate (FAR). The foraminifera to nannofossil AR was then approximated by dividing the CF AR by the FF AR (>63 μm/<63 μm) (see Text S1 for a full equation list). Planktic foraminiferal accumulation rates, in terms of number of specimens (foraminifera #/cm^2/kyr), were calculated from planktic foraminiferal counts in the >150 μm size fraction. The effect of dissolution was assessed using fragmentation data [*Le and Shackleton*, 1992], based on counts of 500 specimens per sample: fragmentation ratio (%) = 100% × (number fragments/8)/(number fragments/8 + number whole).

We determined the relative abundances of benthic foraminiferal taxa and used these to infer changes in carbonate saturation state, oxygenation, and food supply [*Jorissen et al.*, 1995, 2007; *Thomas*, 1998, 2007; *Gooday*, 2003; *Gooday and Jorissen*, 2012; *Foster et al.*, 2013]. Comparisons between past and recent benthic environments need careful evaluation, because Eocene deep-sea benthic foraminiferal assemblages were structured very differently from todays'. For instance, taxa reflecting highly seasonal deposition of organic matter were generally absent or rare, and cylindrically shaped taxa with complex apertures, which are now extinct, were common [e.g., *Thomas and Gooday*, 1996; *Thomas*, 2007; *Hayward et al.*, 2012]. The distribution of these extinct taxa resembles that of buliminids [*Hayward et al.*, 2012], and they were probably infaunal, as confirmed by their δ^{13}C values [*Mancin et al.*, 2013]. The living species *Nuttallides umbonifera* [*Bremer and Lohmann*, 1982] reaches high relative abundances between lysocline and carbonate compensation depth, and we infer that increases in relative abundance of its ancestral species *N. truempyi* similarly correlate with poorly saturated waters, as confirmed by its bathymetric occurrences [*Thomas*, 1998]. Benthic foraminiferal accumulation rates (BFARs) are a proxy for delivery of food to the seafloor and generally are higher at shallower depths [*Herguera and Berger*, 1991; *Jorissen et al.*, 2007]. Benthic foraminiferal accumulation rates were calculated as BFAR = benthic foraminifera (# g^{-1}) × bulk MAR. (A full list of sedimentological and derived accumulation rate definitions and calculations is given in Text S1.)

2.4. Earth System Modeling

We explore some of the possible influences on the sediment record of ETM2, including changes in benthic foraminiferal abundance and bioturbation, using the GENIE Earth system model. GENIE comprises a 3-D ocean circulation model coupled to a 2-D sea ice and atmospheric energy-moisture-balance model plus representation of ocean-sediment-weathering carbon cycling, as summarized by *Archer et al.* [2009]. Continental configuration and climatology, initial ocean chemistry, atmospheric CO_2, and total global weathering flux, are as described by *Ridgwell and Schmidt* [2010]. The model is spun-up for a total of 200,000 years to fully balance marine $CaCO_3$ sedimentation versus weathering and create a sufficient sediment column thickness to support any subsequent $CaCO_3$ "burn-down" [*Ridgwell*, 2007]. The model grid and initial distribution of sedimentary wt % $CaCO_3$ is illustrated in Figure 1a.

To perturb bulk carbonate content and the recording of the δ^{13}C signal, the model was run with a prescribed time history of atmospheric composition. We assumed a gradual doubling of pCO_2 over 45 kyr from 834 ppm [*Ridgwell and Schmidt*, 2010] to 1668 ppm at the peak of ETM2 [*Stap et al.*, 2009], followed by a decline.

Table 1. List of (GENIE) Earth System Modeling Experiments[a]

	Interval: 0–40 ka			Interval: 40–65 ka			Interval: 65–100 ka		
Experiment ID #	Interface Dissolution	Bioturbation	Decreased Saturation	Interface Dissolution	Bioturbation	Decreased Saturation	Interface Dissolution	Bioturbation	Decreased Saturation
STD	Y	Y	N	Y	Y	N	Y	Y	N
STD_sat	Y	Y	N	Y	Y	Y	Y	Y	N
STD_bio	Y	Y	N	Y	N	N	Y	Y	N
STD_satbio	Y	Y	N	Y	N	Y	Y	Y	N
ALT	N	Y	N	N	Y	N	N	Y	N
ALT_sat	N	Y	N	N	Y	Y	N	Y	N
ALT_bio	N	Y	N	N	N	N	N	Y	N
ALT_satbio	N	Y	N	N	N	Y	N	Y	N

[a]Shown are the combination of assumptions of (i) interface dissolution model (otherwise homogeneous); (ii) bioturbation of upper sediment layers (otherwise no vertical mixing); and (iii) reduced carbonate saturation, simulated by increasing the pressure used in calculation carbonate saturation by the equivalent of 2000 m, that are applied to each of three separate phases of the total 100 kyr of model simulation.

Atmospheric CO_2 $\delta^{13}C$ is mirror-imaged and assumes an excursion magnitude of $-1.5‰$ [*Stap et al*., 2009]. We do not aim to reconstruct the history of CO_2 emissions (unlike, e.g., *Kirtland Turner and Ridgwell* [2013]) but instead create and apply to the model a deliberately conceptual time history of atmospheric pCO_2. Doubling of CO_2 in our idealized carbon forcing drives an ~2.9°C warming in mean annual average ocean surface temperatures (~3.0°C in the deep sea)—consistent with available ETM2 temperature proxies [*Stap et al*., 2010a; *d'Haenens et al*., 2014]. The form of prescribed pCO_2 and $\delta^{13}C$ are also chosen such that together, the decline and recovery of $\delta^{13}C$ can be replicated at Site 1262. Note that we do not attempt to explicitly model $\delta^{18}O$, which requires a detailed simulation of atmospheric moisture transport and hence a coupled climate model [e.g., *Tindall et al*., 2010]. Given the similarity between $\delta^{13}C$ and $\delta^{18}O$ ETM2 horizon anomalies, it is unlikely that simulating $\delta^{18}O$ in the model would provide additional constraints.

To explore what factors might help explain the different sedimentological and isotopic ($\delta^{13}C$) observations at Site 1263, we ran permutations of (i) bioturbational mixing occurring continuously throughout the experiment versus discontinuous bioturbational mixing, with bioturbation ceasing during the peak of the event; (ii) "interface" dissolution of carbonate (the default setting in GENIE) versus "homogeneous" dissolution [*Ridgwell*, 2001]; and (iii) no significant ocean circulation change versus reduced bottom water saturation at intermediate water depths (which we crudely simulate by increasing the pressure used in calculating carbonate stability at 1263 by the equivalent of 2000 m water depth), summarized in Table 1. All experiments were run for 100 kyr and sediment cores "extracted" from the model grid [*Kirtland Turner and Ridgwell*, 2013; *Ridgwell*, 2007] at locations corresponding to the Walvis Ridge area (Figure 1a)—one at 1500 m model water depth (the model Site 1263 analogue) and one at 3600 m (analogue to 1262). The chronology for the model cores is created analogous to the observations and assumes a constant terrigenous flux to the sediments, which assumes a fixed globally uniform value of $0.180\,g\,cm^{-2}\,kyr^{-1}$ following *Panchuk et al*. [2008]. We also ran a 100 kyr long control experiment ("CTRL"), in which no atmospheric forcing (or modification of bioturbation or local carbonate saturation) was applied.

3. Results

The reconstructed sedimentation rate for both sites is shown in Figure 3, plotted with sediment lightness, alongside core photos [*Zachos et al*., 2004a, 2004b]. Sedimentation rate at the shallow site was approximately twice the rate at the deep site, with preevent (<20 ka) deposition at Site 1263 averaging 1.96 cm/kyr, compared with 1.08 cm/kyr at Site 1262. From preevent to peak-event values, the former sees an ~12-fold drop in sedimentation rate, the latter a 10-fold decrease.

As noted but not explained by *Stap et al*. [2009], bulk stable isotope records for the two sites show clear differences (Figures 2, 4a, and 4b). At the deeper site, bulk $\delta^{13}C$ values exhibit a gradual decline and then recovery across ETM2. The shallow site, however, also shows a gradual decline/recovery for the start/end of the event but exhibits an additional excursion during the peak phase (ETM2 horizon; ~38–56 ka). The bulk $\delta^{18}O$ record similarly shows a greatly enhanced difference within the ETM2 horizon, with much more

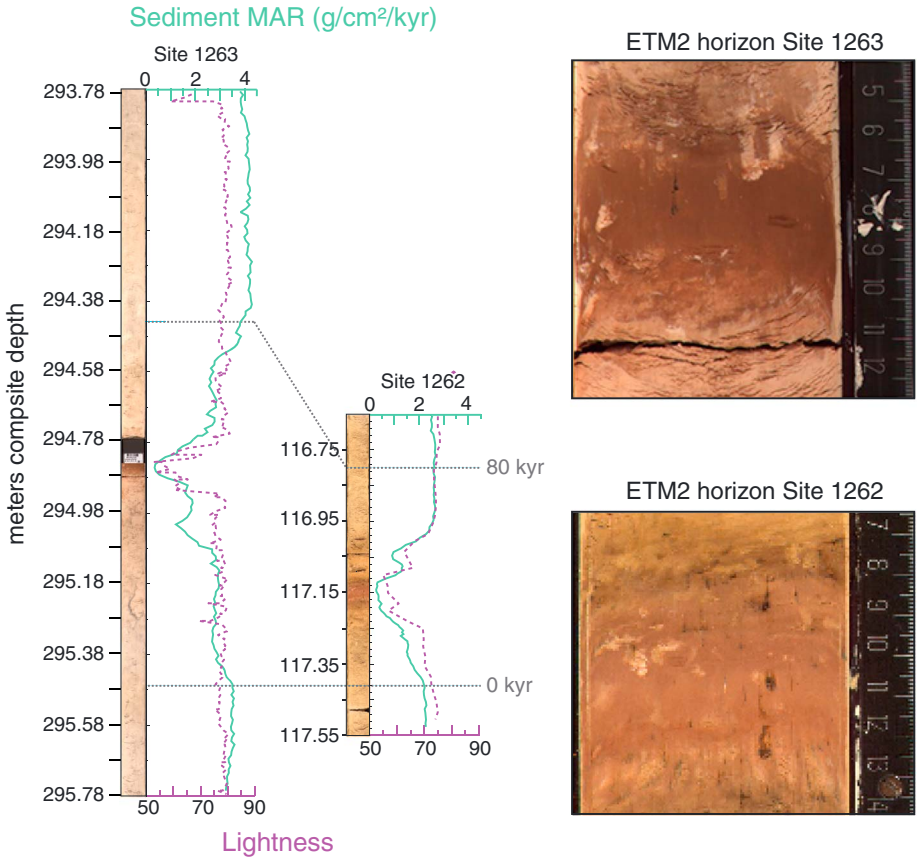

Figure 3. Photographs of sections across the ETM2 event in two cores, from Site 1262 and Site 1263, from Walvis Ridge ODP Leg 208, and the respective approximate sedimentation rates for the two sites, as well as sediment lightness (color [*Zachos et al*., 2004a, 200b]).

negative values at the shallow site, although surface dwelling *Acarinina* records do not follow this trend [*Stap et al*., 2010b]. Intermediate sites along the depth transect, 1265 and 1267 (not shown), are similar to the deep site [*Stap et al*., 2009].

The records of sedimentary $CaCO_3$ content (Figure 4c) share some features of the bulk stable isotope records [*Stap et al*., 2009], in as much as the minimum in $CaCO_3$ wt % at 1263 occurs over a much shorter interval than at 1262, although the minimum $CaCO_3$ wt % values at both sites are similar. Fragmentation (Figure 4h and Table 2) increased at both sites during ETM2, with the pattern largely mirroring that of $CaCO_3$ wt % but noisier, with the increase in fragmentation more gradual and longer lasting at the deep site. Similarly, $CaCO_3$ MAR patterns broadly follow the trend of $CaCO_3$ content, but the $CaCO_3$ MAR was higher at the shallow site by a factor of 1.5–2.0 before and after ETM2. Patterns in coarse fraction (i.e., planktic foraminiferal) MAR, susceptible to dissolution and thus indicative of corrosiveness, resemble $CaCO_3$ MARs, and thus FF MAR, despite its minor contribution to the sediment (Figure 4e and Table 2). Planktic foraminiferal accumulation rates (PFARs—Figure 4g) at both sites were identical prior to the events but differed during the interval when $CaCO_3$ wt % remained even at Site 1263 while declining at 1262. The differential changes between the foraminiferal and the coccolithophore response result in relative increases in the foraminiferal contribution to the bulk carbonate at the shallow site between about 16 and 38 ka (Figure 4f and Table 2), the interval just before the peak of ETM2.

Benthic foraminiferal parameters generally resemble sedimentary records. Benthic foraminiferal accumulation rates (BFARs—Figure 5a) at each site were similar before and after the event, with overall slightly higher values at the shallower site. At both sites, BFAR started to decline gradually at the start of ETM2 but more pronouncedly at the deeper site. During start and recovery, the difference in BFAR between the two sites was significantly higher than during background conditions, but during peak ETM2

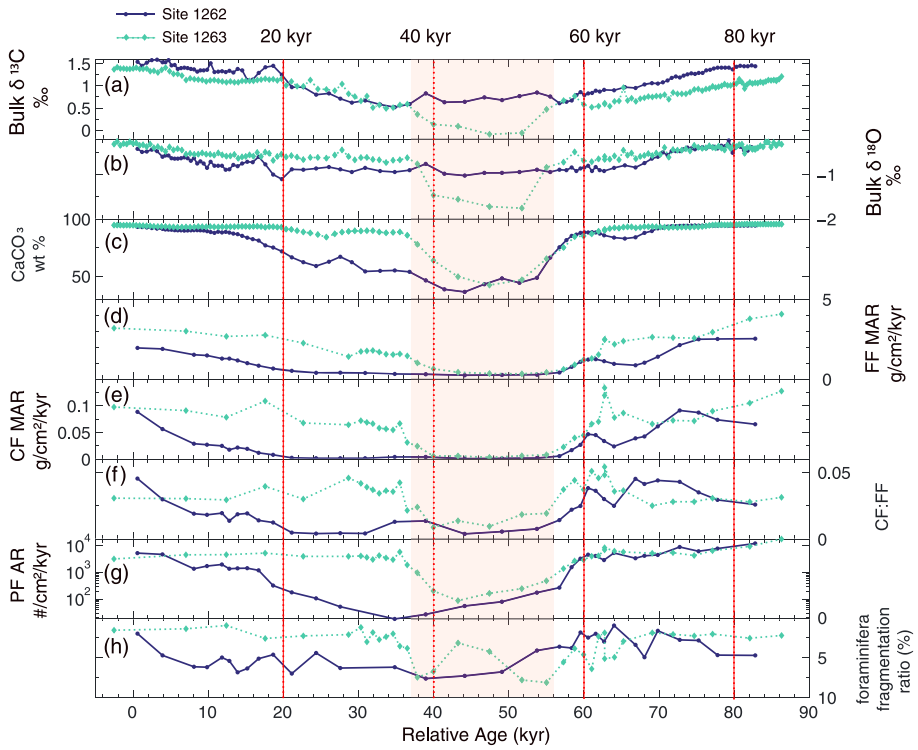

Figure 4. Sedimentary response to ETM2: (a) bulk $\delta^{13}C$, (b) bulk $\delta^{18}O$, (c) $CaCO_3$ wt % [*Stap et al.*, 2009], (d) fine fraction (<63 μm) mass accumulation rate (FF MAR), (e) coarse fraction (>63 μm) mass accumulation rate, (f) ratio of fine fraction MAR/coarse fraction MAR, (g) planktic foraminiferal accumulation rate (PF AR), and (h) foraminifera fragmentation ratio (%).

(40–55 ka), BFAR values at Site 1263 declined precipitously, below those at Site 1262 (Figure 5a and Table 4). Samples were essentially barren of benthic foraminifera [*Stap et al.*, 2010b]. All species-specific ARs declined (Figure S1 in the supporting information and Table 5). No species bloomed during ETM2: all declined in abundance, though some more than others. The diversity (rarefied number of species) declined parallel to BFAR, with largest differences between the sites during the start (and recovery) phase when values at the shallower site remained relatively high while those at the deep site had started to decline (and had not yet recovered) (Table 4).

Benthic foraminiferal assemblages during background conditions were diverse, with 133 taxa recognized, 117 at the deep site (18 not present at 1263), and 116 at Site 1263 (17 not present at Site 1262) (Data Set S1 in the supporting information). The number of species (rarefied to 100 specimens) was higher at the shallow site (background values of 41 species) than at the deep site (33 species) (Figure 5b), largely due to the presence of diverse species of *Lenticulina* and other lagenid species. *Nuttallides truempyi* was the most common species at both sites, with *Oridorsalis umbonatus*, *Quadrimorphina profunda*, *Bulimina kugleri*, and *Bulimina simplex* (Table 3). Species present at the shallow site only include *Cibicidoides alleni* and *C. laurisae*

Table 2. Absolute Average Values of Sediment Core Characteristics, Split Into 20 kyr Time Periods, With 40–60 kyr Equating to the Height of the ETM2 Event

	1263					1262				
	<20 kyr	20–40 kyr	40–60 kyr	60–80 kyr	>80 kyr	<20 kyr	20–40 kyr	40–60 kyr	60–80 kyr	>80 kyr
Carbonate AR (g/cm^2/kyr)	2.811	1.362	0.475	2.058	3.831	11.160	0.232	0.394	1.426	2.45
Fine fraction AR (g/cm^2/kyr)	2.905	1.548	0.624	2.165	3.922	1.309	0.392	0.514	1.503	2.380
Coarse fraction AR (g/cm^2/kyr)	0.094	0.053	0.019	0.078	0.116	0.031	0.003	0.009	0.055	0.066
CF AR/FF AR	0.033	0.033	0.026	0.038	0.030	0.021	0.007	0.013	0.037	0.028
Planktic foraminifera AR (#/cm^2/kyr)	4482	3271	1200	5367	13846	2123	78	927	5309	12313
Fragmentation ratio (%)	1.64	3.27	5.35	3.20	2.40	5.24	6.31	4.58	2.88	4.72

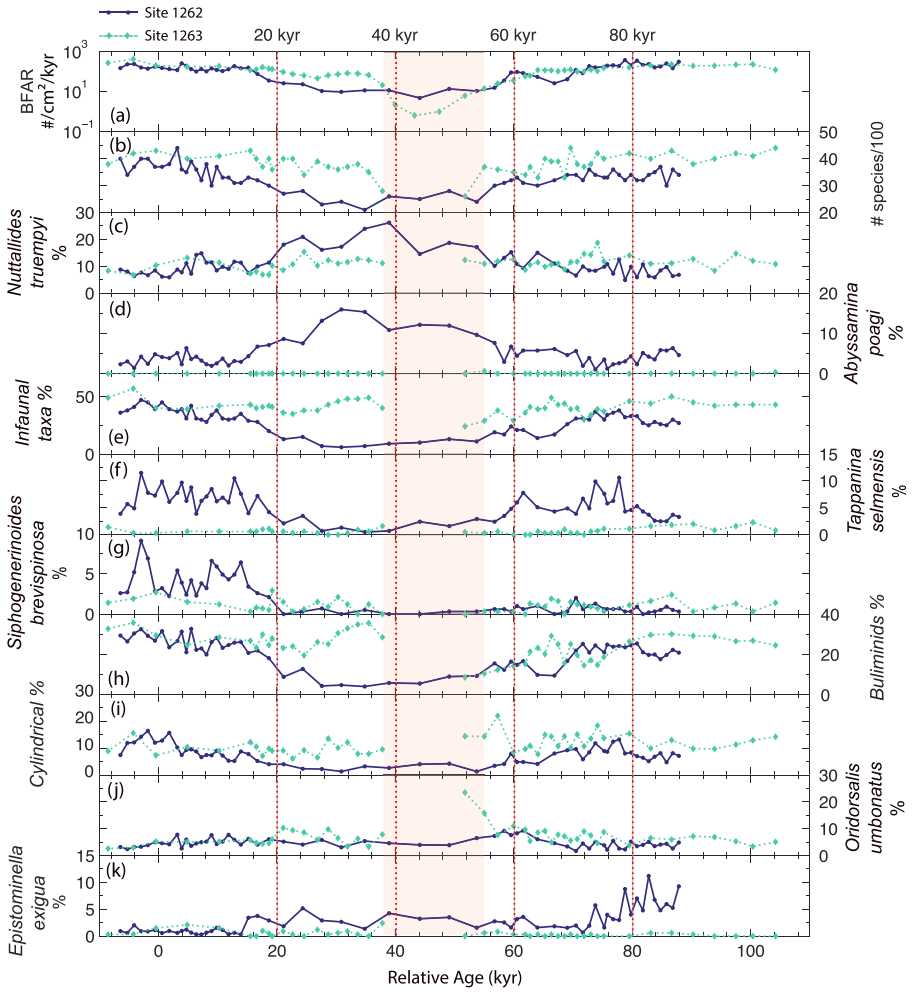

Figure 5. Biological response to the ETM2: (a) benthic foraminifera accumulation rate, BF AR; (b) rarefied number of species (/100); and (c–j) % abundance of individual benthic foraminifera species. Site 1263 % abundances are not plotted during the peak event, because very few specimens were present (Data Set S1).

and the agglutinant *Vulvulina jarvisae*, as well as several uniserial lagenid species. Those present at the deep site only include mainly agglutinant species (e.g., *Repmanina charoides*, *Trochamminoides serpens*, and *Siphotextularia rolszhauseni*). All species present at one site only are rare (<0.5 of total assemblage).

During ETM2, *Nuttallides truempyi* and *N. umbonifera* increased in relative abundance (Figure 5c) at the deep site, as did *Abyssamina poagi*, *Globocassidulina subglobosa*, and *Cibicidoides* species, whereas *Tappanina selmensis* and *Siphogenerinoides brevispinosa*, probably opportunistic infaunal taxa [*Steineck and Thomas*, 1996; *Thomas*, 1998, 2003], decreased in relative abundance (Figures 5d, 5f, and 5g). Epifaunal species thus overall increased in relative abundance at the deep site, and infaunal species decreased (Figure 5e) during the full duration of ETM2. In contrast, at the shallow site, infaunal taxa as a whole and the generally infaunal buliminid and cylindrical species remained equal or increased somewhat in relative abundance during the start of ETM2, so that the difference in relative abundances at the two sites increased (Figures 5e, 5h, and 5i). A similar difference developed during the recovery phase. In addition, the shallow infaunal *Oridorsalis umbonatus* [*Thomas and Shackleton*, 1996] increased in relative abundance at the shallow site just after the peak event (Figure 5j). During the peak event benthic foraminifera were essentially absent at Site 1263. After the peak event and extending after the recovery phase, agglutinant taxa at the deep site remained less abundant, as did *Siphogenerinoides brevispinosa*. *Epistominella exigua* became more common after ETM2, and *Quadrimorphina profunda* did so at the shallow site (e.g., Figures 5g and 5k).

Table 3. Most Common Taxa at Sites 1262 and 1263, as Percentage of the Total Number of Specimens Counted Over All Samples at That Site[a]

Site 1262	%	Site 1263	%
Nuttallides truempyi	10.5	*Nuttallides truempyi*	10.9
Quadrimorphina profunda	9.5	*Bulimina simplex*	7.7
Nuttallides umbonifera	6.2	*Abyssamina incisa*	7.4
Bulimina kugleri	5.8	*Oridorsalis umbonatus*	6.7
Tappanina selmensis	5.5	*Bulimina kugleri*	5.3
Abyssamina poagi	5	*Clinapertina complanata*	3.9
Clinapertina complanata	5	*Globocassidulina subglobosa*	3.5
Oridorsalis umbonatus	4.8	*Abyssamina* sp.	3.3
Anomalinoides spissiformis	4.2	*Pleurostomella acuminata*	3
Fursenkoina fusiformis	3.1	*Lenticulina muensteri*	2.9
Epistominella exigua	2.8	*Fursenkoina fusiformis*	2.6
Pleurostomella acuminata	2.8	*Clinapertina inflata*	2.4
Nonionella robusta	2.4	*Nonion havanense*	2.3
Globocassidulina subglobosa	2.4	*Siphonodosaria lepidula* s.l.	2.2
Clinapertina inflata	2.3	*Bulimina semicostata*	2.2
Siphogenerinoides brevispinosa	2	*Anomalinoides spissiformis*	2.2
Abyssamina incisa	1.9	*Aragonia aragonensis*	2.1
Abyssamina quadrata	1.8	*Cibicidoides mundulus* group	1.9
Nonion havanense	1.8	*Nuttallides umbonifera*	1.7
Bolivinoides huneri	1.6	*Nonionella robusta*	1.6
Cibicidoides mundulus group	1.5	*Vaginulina elegans*	1.4
Bulimina simplex	1.4	*Laevidentalina communis*	1.2
Anomalinoides sp. cf. *acutus*	1.4	*Quadrimorphina profunda*	1.2
Abyssamina sp.	1.3	*Bulimina trinitatensis*	1.1
Gyroidinoides mediceus	1	*Alabamina dissonata*	1
		Siphogenerinoides brevispinosa	1
		Stilostomella aculeata	1

[a]The 27 species listed for Site 1263 and the 25 species listed for Site 1262 are present at 1% or more of that total population; all other taxa are less abundant.

4. Discussion

The biotic and sedimentary records across ETM2 at Walvis Ridge are striking in their similarity. Both record more gradual change at the deeper site, with a generally more extreme and much shorter superimposed change during the peak of the event at the shallower site only. If CO_2 addition and associated decline in carbonate saturation alone were driving the sedimentary observations, we would have expected a sharper wt % $CaCO_3$ response at 1262 compared to 1263 because of the lower initial saturation and hence lower fractional carbonate preservation at greater depth [*Stap et al*., 2009]. Assuming a similar ocean acidification (carbonate ion decline) at all depths, the nonlinear nature of the wt % $CaCO_3$ scale means that at lower initial wt % $CaCO_3$, only a relatively small decline in carbonate preservation is needed to produce a large change in wt %. Instead, we observe the opposite, i.e., a sharper response at the shallow site, which starts at higher wt % $CaCO_3$. There is no indication of unconformities (Figure 3) [*Stap et al*., 2009] bracketing the ETM2 horizon and hence no indication of a removal of most of the onset and recovery at Site 1263 to explain the sharp transitions. We also discard the possibility of sampling biases. *Stap et al*. [2009] sampled 1262 more closely spaced (at 0.5 cm) within the ETM2 horizon. Hence, wt % $CaCO_3$, $\delta^{13}C$, and $\delta^{18}O$ (Figures 4a–4c) measurements are more closely spaced in time at the deep site, implying that the smoother bulk carbonate composition trends at 1262 cannot be due to a sampling artifact. If anything, the less frequent sampling in depth (thus time) across the ETM2 horizon at 1263 could have underestimated the abruptness of the transition into and out of peak ETM2 conditions. We also rule out sampling differences as an explanation for the absence of benthic foraminifera at 1263. Unlike the bulk carbonate records, sampling for benthic foraminiferal analysis was regular (2 cm). The difference in sedimentation rates, which prior to ETM2 averaged 1.08 cm/kyr at the deep site compared with 1.96 cm/kyr at the shallow site, hence leads to a higher frequency in time of sampling at 1263 versus 1262. It is extremely unlikely that the presence of foraminifera during the ETM2 horizon was missed in the more frequently sampled (in time) core.

Table 4. Average Values of Number of Species, Total Benthic Foraminifera Accumulation Rate (BFAR), and Relative Abundances of Individual Benthic Foraminifera Species During the ETM2[a]

	Percent of the Population									
	1263					1262				
	<20 kyr	20–40 kyr	40–60 kyr	60–80 kyr	>80 kyr	<20 kyr	20–40 kyr	40–60 kyr	60–80 kyr	>80 kyr
Rarefied number of species (100)	40	36.4	33.5	38.29	41.14	35.54	24.83	28.33	38.29	41.14
A. poagi %	0	0	0.15	0	0.04	3.63	11.87	8.47	0	0.04
Q. profunda %	0.77	1.06	1.19	0.86	2.76	4.78	9.41	10.01	0.86	2.76
Clinapertina %	5.49	6.68	10.23	6.95	4.78	14.06	20.38	10.83	6.95	4.78
N. truempyi %	8.91	11.54	11.91	11.94	11.49	9.28	7.57	14.79	11.94	11.49
N. umbonifera %	1.04	1.46	1.72	1.94	2.78	7	7.57	8	1.94	2.78
N. truempyi and *N. umbonifera* %	9.95	12.85	13.64	13.88	14.28	4.21	24.58	22.8	13.88	14.28
A. aragonensis %	2.28	1.22	0.89	2.97	1.82	25.96	1.57	0.19	2.97	1.82
T. selmensis %	0.7	0.52	0.35	0.47	1.55	7	1.46	2.93	0.47	1.55
S. brevispinosa %	1.4	0.93	0.22	0.97	1.15	4.21	0.25	0.36	0.97	1.15
Buliminids %	28.44	28.11	11.49	20.48	28.05	25.96	6.8	11.43	20.48	28.05
Agglutinants %	1.13	0.93	0.15	1.35	1.18	1.67	1.81	1.98	1.35	1.18
Lenticulina spp. %	5.21	5.15	3.88	5.85	4.95	0.06	0.05	0.05	5.85	4.95
Lagenids %	2.73	2.62	2.38	3.76	2.13	4.82	0.92	0.21	3.76	2.13
Cibicidoides spp %	3.41	3.22	2	3.31	3.57	2.05	4.76	3.84	3.31	3.57
S. rugosa %	0.34	0.06	0	0.47	0.25	9.22	0.66	0.05	0.47	0.25
O. umbonatus %	4.67	7.14	14.5	7.03	5.78	4.82	4.7	6.43	7.03	5.78
G. subglobosa %	4.32	3.1	1.91	3.91	2.88	1.15	5.06	3.82	3.91	2.88
Cylindrical taxa %	9.99	9.2	14.78	12.82	11.51	9.22	2.6	4.16	12.82	11.51
Buliminids and cylindrical taxa %	38.43	37.31	26.27	33.31	39.56	35.18	9.4	15.59	33.31	39.56
E. exigua %	0.71	0.69	0.44	0.11	0.22	1.15	3.03	2.52	0.11	0.22
BFAR	201.62	63.71	15.02	116.22	207.5	61.59	13.78	29.35	116.22	207.5

[a]The event is split into 20 kyr time periods.

4.1. Benthic Foraminiferal Response to the ETM2

In general, the most diverse benthic assemblages, with cooccurring epifaunal and infaunal dwellers, are indicative of intermediate food availability. When little particulate organic carbon arrives at the seafloor, there is insufficient food to sustain infaunal populations, and at extreme food abundance, oxygen levels in pore waters (and finally in bottom waters) become too low to sustain infaunal populations [*Jorissen et al.*, 2007]. The relative abundance of infaunal taxa thus is a proxy for increased food supply and/or declining oxygen levels.

At the deep site, BFAR as well as relative abundance of infaunal taxa (buliminids and cylindrical taxa) declined gradually to reach the lowest levels for that site during the peak event, before increasing again (Figure 5 and Tables 4 and 5). Relative abundances of *N. truempyi* and *N. umbonifera*, indicative of undersaturated bottom waters and/or oligotrophic conditions [*Bremer and Lohmann*, 1982; *Thomas*, 1998], increased, as did that of the abyssaminids. The latter are extinct but were generally more abundant at greater depths [e.g., *Thomas*, 1998], thus probably indicative of oligotrophic conditions. All benthic foraminiferal indicators point to a declining food supply to the seafloor during ETM2 at Site 1262. In contrast, calcareous nannofossil evidence for nearby Site 1265 does not indicate significant changes in productivity in the region [*Dedert et al.*, 2012].

Can indicators of relatively unchanging surface productivity be reconciled with an interpretation of declining benthic food supply? It is unlikely that the strong decrease in BFAR and diversity is driven by taphonomic dissolution only, because the proportion of *Abyssamina poagi*, a small, smooth, dissolution-prone taxon, increased during peak ETM2, i.e., maximum dissolution (Figure 5c), whereas dissolution would have led to a relative increase in relatively large, heavily calcified taxa [e.g., *Nguyen et al.*, 2009; *Nguyen and Speijer*, 2014]. Instead, we suggest that temperature changes associated with ETM2 are key. Higher temperatures influence biological processes [*Pörtner et al.*, 2014] due to their effect on enzyme reactions, diffusion, and membrane transport [*Hochachka and Somero*, 2002], increasing metabolic rates [*Hoegh-Guldberg and Bruno*, 2010]. Temperature-driven increased metabolic rates at a constant food supply would by themselves produce an energy deficit. In addition, warmer oceans might see a greater degree of remineralization of organic matter in the water column [*O'Connor et al.*, 2009], a possibility,

Table 5. Average Values of Species-Specific Benthic Foraminifera Accumulation Rate (BFAR) During the ETM2[a]

	Species-Specific Benthic Foraminifera Accumulation Rates									
	1263					1262				
	<20 kyr	20–40 kyr	40–60 kyr	60–80 kyr	>80 kyr	<20 kyr	20–40 kyr	40–60 kyr	60–80 kyr	>80 kyr
A. poagi AR	0.000	0.000	0.042	0.000	0.641	0.525	0.016	0.053	0.612	0.596
Q. profunda AR	3.469	0.810	0.183	1.132	0.844	0.385	0.020	0.036	0.147	0.254
Clinapertina AR	0.374	0.108	0.015	0.180	0.476	0.119	0.023	0.032	0.275	0.330
N. truempyi AR	0.244	0.057	0.012	0.100	0.184	0.180	0.008	0.020	0.192	0.339
N. umbonifera AR	3.049	0.571	0.086	0.724	0.929	0.233	0.036	0.033	0.282	0.367
N. truempyi and *N. umbonifera AR*	0.218	0.051	0.011	0.085	0.147	0.413	0.004	0.012	0.108	0.171
A. aragonensis AR	1.058	1.144	0.141	0.711	1.265	0.058	0.073	0.098	0.599	0.722
T. selmensis AR	4.136	1.112	0.184	2.088	1.457	0.233	0.144	0.085	0.270	0.713
S. brevispinosa AR	1.902	0.671	0.465	1.233	3.149	0.413	0.204	0.773	3.014	5.120
Buliminids AR	0.069	0.023	0.012	0.059	0.074	0.058	0.024	0.022	0.072	0.114
Agglutinants AR	3.520	0.703	0.305	1.178	1.623	1.533	0.155	0.161	1.093	1.887
Lenticulina spp. AR	0.410	0.129	0.038	0.236	0.431	1.069	0.061	0.194	1.283	2.997
Lagenids AR	0.841	0.268	0.062	0.348	1.972	0.371	0.070	0.406	1.253	1.488
Cibicidoides spp AR	0.817	0.316	0.086	0.362	0.713	0.880	0.039	0.073	1.047	2.542
S. rugosa AR	1.353	0.574	0.000	2.126	0.594	0.177	0.011	0.194	1.951	3.855
O. umbonatus AR	0.513	0.104	0.014	0.183	0.382	0.371	0.035	0.042	0.480	0.604
G. subglobosa AR	0.549	0.227	0.082	0.374	0.839	2.108	0.047	0.096	1.758	1.544
Cylindrical taxa AR	0.204	0.073	0.012	0.094	0.185	0.177	0.063	0.064	0.185	0.378
Buliminids and cylindrical taxa AR	0.051	0.017	0.006	0.035	0.052	0.043	0.017	0.016	0.051	0.087
E. exigua AR	3.422	1.071	0.316	1.365	1.939	2.108	0.064	0.153	0.571	0.364
Infaunal taxa AR	0.045	0.015	0.005	0.029	0.047	0.043	0.017	0.016	0.051	0.087

[a]The event is split into 20 kyr time periods.

e.g., demonstrated for the Eocene of offshore Tanzania on the basis of reconstructed water column $\delta^{13}C$ gradients [*John et al.*, 2014]. Increased metabolic rates combined with increased remineralization of organic matter in the water column lead to a lesser arrival of food at the seafloor despite constant productivity [*Ma et al.*, 2014] and could, coupled with the highly food-limited nature of benthic foraminifera in today's oceans [*Linke*, 1992], explain the strongly reduced BFARs.

Faunal changes were more complex at the shallower site, despite the fact that the sites are relatively close to each other and hence under waters with similar primary productivity [*Zachos et al.*, 2004a, 2004b]. Whereas BFAR, species diversity, and buliminid taxa all decreased simultaneously during the early and recovery phases of ETM2 at the deep site, the relative abundance of buliminid taxa at the shallow site increased, despite decreasing BFAR and species diversity (Figure 5). Several infaunal taxa decreased in relative abundance at Site 1263 during the peak ETM2 (e.g., *S. brevispinosa* and *T. Selmensis*; Figures 5f and 5g), suggesting that these taxa were less able to survive the lowered food supply at this site, indicated by the more severe drop in BFAR, than other infaunal taxa such as buliminids. In contrast, these species decline similarly to buliminids at Site 1262. During the recovery phase, the relative abundance of the shallow infaunal *O. umbonatus* increased; this increase was likely not caused by an increase in food supply, because the BFAR remained low relative to preevent values. Buliminid taxa and *O. umbonatus* % increased in relative abundance just prior to the peak event (20–40 kyr). Both calcify in the less saturated pore waters rather than in bottom waters, so the increase might have been caused by increasing undersaturation [*Foster et al.*, 2013], but this does not agree with the observation that at the shallow site, the carbonate parameters ($CaCO_3$ wt %, fragmentation, and PFAR) remained constant during the interval with increased abundance of buliminid taxa. This increased abundance of buliminid taxa and *O. umbonatus* during declining food levels and invariant carbonate corrosiveness thus indicates that oxygenation was declining in bottom and/or pore waters at the shallow site, possibly due to rising temperatures, increased remineralization of organic matter, or changes in preformed oxygen levels due to changes in ocean circulation pattern.

During the peak phase of ETM2, benthic foraminifera were absent at Site 1263, indicating that bottom and pore water conditions could not support them, and were less favorable than at the deeper Site 1262 where benthic foraminifera remained present. Deoxygenation was more severe and persisted longer at the

seafloor at Site 1263 than at Site 1262 during the PETM at the Walvis Ridge based on bulk sediment trace element data [*Chun et al*., 2010; *Pälike et al*., 2014] and mineralogical data [*Post et al*., 2015]. A similar occurrence during ETM2 would help explain the differential benthic assemblage changes between Sites 1262 and 1263. Benthic foraminiferal records during the PETM cannot be compared between the sites because of the severe carbonate dissolution during the peak PETM, with $CaCO_3$ fully dissolved for part of the PETM at all sites, longer at the deeper sites [*Zachos et al*., 2005].

4.2. Ocean Circulation as a Driver of Depth-Specific Ecological Change

We interpret our observations in terms of a change in the source of intermediate waters bathing Site 1263, driving a much larger warming and decrease in dissolved oxygen compared to 1262. Support for this comes from the results of Paleocene/early Eocene fully coupled atmosphere-ocean climate general circulation model experiments [*Lunt et al*., 2010]. These experiments demonstrate that an atmospheric CO_2 and surface warming threshold could exist, beyond which any further CO_2 rise and surface warming lead to a disproportionately larger increase in temperature increase in the intermediate waters than in the deep ocean. For instance, in the simulations of *Lunt et al*. [2010], going from $2\times$PAL to $6\times$PAL CO_2, where PAL is 280 ppmv, produced a warming of 1.7°C at 1500 m compared to 0.2°C at ~3500 m (Figure 6). All other things being equal, a change in water mass source and/or mixing that leads to higher local temperatures will be associated with lower dissolved O_2, although the specific pathway and hence integrated remineralization of organic matter along that pathway will also affect the local value of $[O_2]$.

A change in circulation during ETM2 has also been suggested by *d'Haenens et al*. [2014], inferred from a short-lived reversal of meridional $\delta^{13}C$ gradients of 0.50–1.00‰ between the North and South Atlantic (Deep Sea Drilling Project Sites 401 and 550, NE Atlantic and the Walvis Ridge sites, respectively). Similarly, ocean circulation change has been inferred at Site 1263 during the PETM as implied by the largest CIE (−3.5‰) in deep-sea benthics, although comparison with the other sites is not possible due to the severe dissolution [*McCarren et al*., 2008]. Direct evidence for a circulation change-driven warming does not yet exist however. Although a 3°C warming during ETM2 was estimated from benthic foraminifera at 1262 [*Stap et al*., 2010a], the relative temperature change at the shallower site is not recorded due to the absence of benthic foraminifera during the critical interval.

4.3. Origins of the "Anomalous" Bulk Sediment Response During Peak ETM2 Conditions

We suggest that the Site 1263 phenomena: (1) a sharp excursion in wt % $CaCO_3$ together with bulk carbonate $\delta^{13}C$ and $\delta^{18}O$ that constitutes the ETM2 horizon and (2) temporary exclusion of benthic foraminifera are causally linked, via the impact of changes in the benthic foraminiferal contribution to bioturbation [*Grosse*, 2002]. We infer that sediment mixing by benthic foraminifera would have effectively ceased at the shallow site during the peak of ETM2. Changes in bottom water conditions would have also affected other benthic biota (including burrowers) because animals are more severely affected by deoxygenation than protists such as foraminifera [*Gooday et al*., 2010]. Surface sediment mixing thus may have ceased during the peak of ETM2 at the shallow site, but not at the deep site, as may be seen in the core photographs, and in the larger and more abrupt change in sediment color (lightness) (Figure 3). This is important, as mixing reduces the recorded magnitude and increases the apparent duration of a signal [*Ridgwell*, 2007; *Kirtland Turner and Ridgwell*, 2013]. Indeed, numerical modeling of hyperthermal events illustrates that a sharper onset to low carbonate content sediments is observed in the absence of bioturbation [*Ridgwell*, 2007; *Kirtland Turner and Ridgwell*, 2013]. An enhanced degree of carbonate dissolution in the ETM2 horizon at 1263 might also have played a role, as the temporary emplacement of a less well ventilated intermediate water mass would be expected to have higher respired dissolved CO_2 concentrations and hence lower saturation. We turn to the Earth system modeling experiments (Table 1) to explore this further.

We first test whether the assumed atmospheric perturbation (Figure 7a) can produce a sediment record consistent with observations from the deep site, where we expect a relatively straightforward and predictable response to ETM2 ocean acidification. In experiment "STD" (Table 1), we simulate a reduction in carbonate content to around 50 wt % in response to increasing atmospheric CO_2 followed by an initially more rapid recovery (Figure 5b), qualitatively consistent with trends observed at Site 1262. Toward the end of the simulation, the modeled sediment record displays an "overshoot" in carbonate content which is also expected [*Dickens et al*., 1997; *Zachos et al*., 2005; *Kump et al*., 2009], although in this specific model

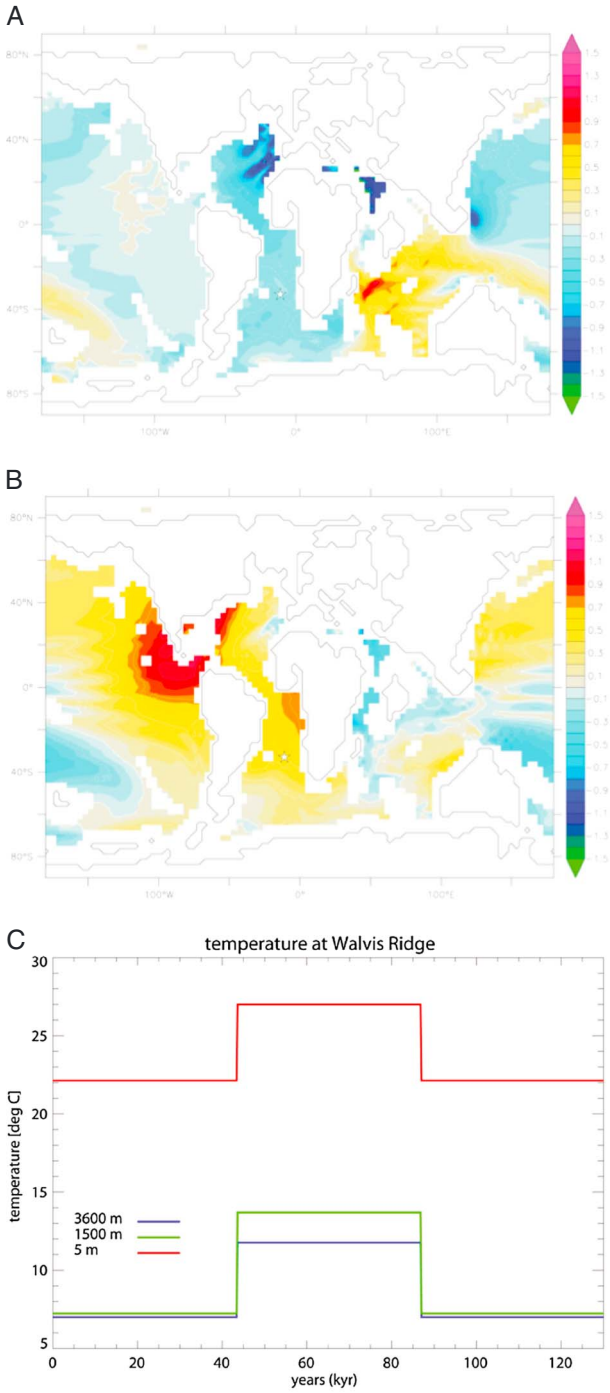

Figure 6. Modeled increase in temperature at intermediate depths (~1500 m) minus the increase in temperature in the deep ocean (~3500 m), given an increase in atmospheric CO_2 from (a) 1 × PAL (preindustrial levels of atmospheric CO_2) to 2 × PAL and (b) 1 × PAL to 6 × PAL. Figure 6b has been scaled to a doubling of CO_2 by multiplying a factor of 0.39. The stars show the approximate paleolocation of the Walvis Ridge site (−11° longitude × −33° latitude). The simulations are from *Lunt et al.* [2010]. In the absence of a circulation switch (Figure 6a), at Walvis Ridge the warming is greater in the deep ocean than in intermediate waters, whereas with a circulation switch (Figure 6b), the warming is in intermediate waters than in the deep ocean. (c) Conceptual evolution of temperature at the Walvis Ridge site through ETM2, from the model simulations of *Lunt et al.* [2010]: temporal evolution of temperature at the surface (~5 m depth), intermediate depths (~1500 m), and the deep ocean (~3500 m). It is assumed that the temperature is that of the 2 × PAL simulation between 0 and ~40 kyr, then (following a circulation switch) the temperature can be characterized by that of the 6 × PAL simulation for a period of ~40 kyr, then the temperature reverts to the preswitch state. The warming following the circulation switch is greater at intermediate depths than in the deep ocean.

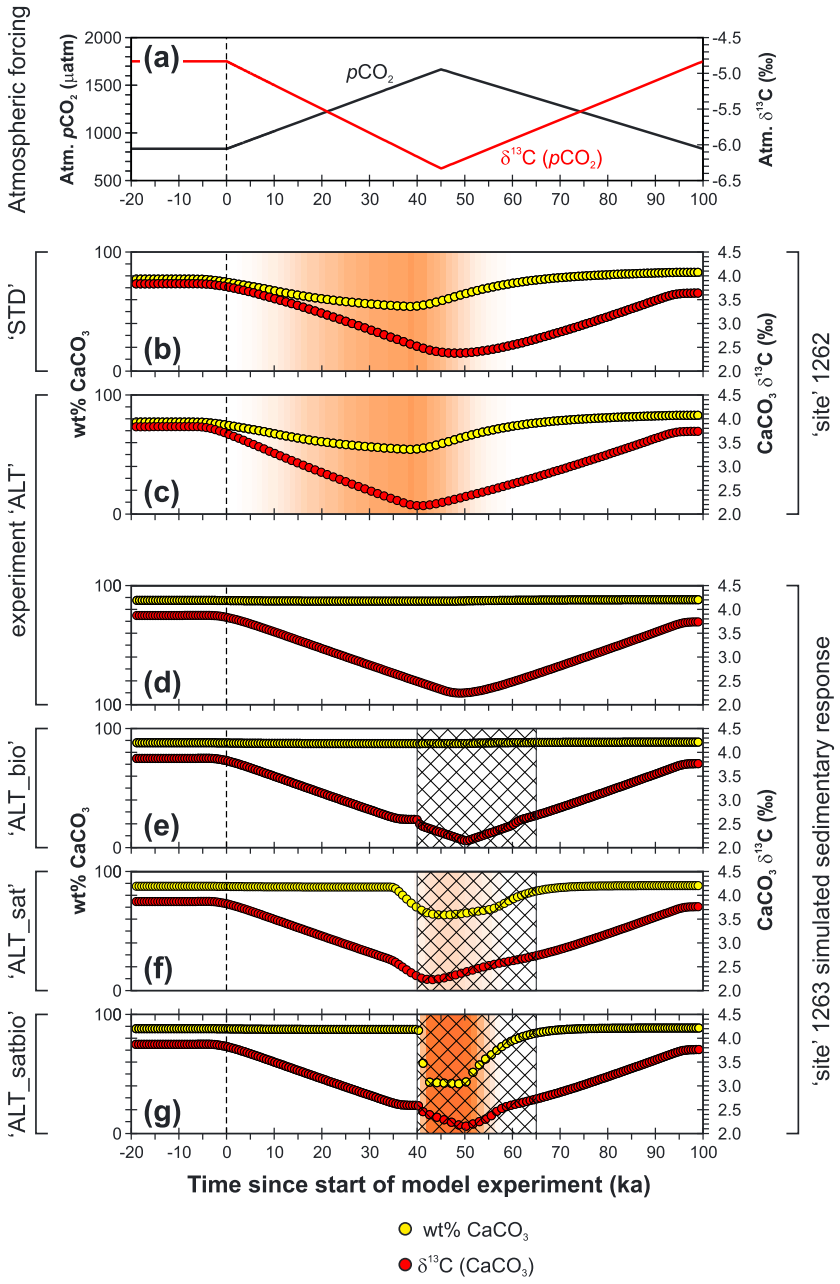

Figure 7. Model-predicted bulk sediment responses. Experiments show bioturbational mixing, interface dissolution occurring but no changing saturation state (STD), the same conditions with no interface dissolution (ALT), and derivatives of this experiment with only a saturation state decrease during the peak event (ALT_sat), with only a shutdown of bioturbation during the peak event (ALT_bio) and a decreased of both bioturbation and saturation state during the peak event (ALT_satbio). (a) The forcing applied to atmospheric CO_2 (LH axis) and to atmospheric $\delta^{13}C_{(CO2)}$ (RH axis). The model time scale runs from 20 kyr prior to the start of the perturbation experiments (i.e., the last 20 kyr of the 200 kyr spin-up) and forward 100 kyr to the model experiment end. Time is plotted relative to the start of the experiment—nominally equivalent to the onset of the ETM2 event (Figure 2) with 0 kyr indicated by a vertical line. (b–g) The predicted evolution of bulk properties, with wt % $CaCO_3$ (yellow symbols) on the LH axis and $\delta^{13}C$ (red symbols) on the RH axis. The background color provides a qualitative illustration of changing carbonate content (white = high wt % $CaCO_3$ and red-brown = low wt % $CaCO_3$). Of these, Figures 7b and 7c show the simulated response at the model equivalent location to Site 1262 and in Figures 7d–7g, for Site 1263. In Figures 7e–7g, the hatched region indicates the interval throughout which there was no bioturbation (mixing) of the upper sediment layers in the model and/or a greater pressure was assumed in calculating carbonate saturation (the 40–65 ka interval in Table 1).

example, it occurs due to a forced removal of CO_2 from the atmosphere (Figure 7a) rather than via an explicit calculation of silicate weathering feedback [*Colbourn et al*., 2013]. Carbonate $\delta^{13}C$ (Figure 5b) exhibits an excursion size slightly less than the applied −1.5‰ magnitude of the forcing (Figure 5a), also as expected [*Kirtland Turner and Ridgwell*, 2013]. However, the $\delta^{13}C$ minimum lags that of wt % $CaCO_3$ by about 10 kyr, whereas in the Site 1262 observations (Figures 4a and 4c), they are approximately synchronous. In experiment "ALT," we hence substitute a homogeneous carbonate dissolution model for the default interface assumption [*Ridgwell*, 2001], so that newly deposited carbonate is mixed into the surface sediment layer before carbonate is removed through dissolution. This brings the $\delta^{13}C$ and wt % $CaCO_3$ minima into alignment (Figure 7c), producing a better match to the Site 1262 observations. (In the interface model of carbonate dissolution, a $\delta^{13}C$ signal from the surface cannot be imprinted on the sediments once the total dissolution flux exceeds the rain flux.) However, little change in wt % $CaCO_3$ is recorded at the analogue location to Site 1263 (Figure 7d). In addition, the simulated $\delta^{13}C$ record at 1263 is too regular and exhibits none of the abrupt transitions characterizing the observed transition into and out of the ETM2 horizon (Figures 3 and 4). In experiments "ALT_bio," "ALT_sat," and "ALT_satbio," we hence explore the possible impact of reduced carbonate saturation, reduced bioturbation, and both together (Table 1).

The temporary cessation of sediment mixing on its own (ALT_bio) at 1263 does little more than introduce small step-like features in the simulated evolution of bulk carbonate $\delta^{13}C$ (Figure 7d), with little noticeable impact on wt % $CaCO_3$. In contrast, temporarily decreasing carbonate saturation on its own (ALT_sat) reduces wt % $CaCO_3$ toward observed Site 1262 values (Figures 7c and 7f). The transitions in bulk composition occur relatively rapidly, to create a simulated feature more reminiscent of the ETM2 horizon (Figure 4c). Combining both temporary saturation decline and cessation of bioturbation (ALT_satbio) leads to a more sharply defined wt % $CaCO_3$ anomaly, particularly with respect to the transition into the peak of the event (Figure 7g). However, only small steps occur in $\delta^{13}C$.

Although not successful in reproducing all the observations, these simple experiments reveal the potential processes associated with specific sedimentary features. First, we find that a change in water mass saturation appears to be key to reproducing the magnitude of anomalous decline and recovery in wt % $CaCO_3$ at Site 1263. That said, we cannot rule out the possibility that the GENIE model does not exhibit an appropriate sensitivity of carbonate preservation to CO_2 addition, particularly as a function of ocean depth. Although outside the scope of this particular paper, the model response to ETM2 could be assessed by contrasting the changes in $CaCO_3$ across the event (Figures 1a and 1b) at multiple sites spanning different ocean basins (e.g., as in *Panchuk et al*. [2008]) and the applied forcing refined, perhaps by means of formal inversion [*Kirtland Turner and Ridgwell*, 2013]. In contrast to reduced saturation, the importance of bioturbation is apparent in dictating the details of the recorded shape of the signal. Only by stopping mixing (bioturbation) between model sediment layers can a sharp decline at the onset of the ETM2 horizon be reproduced. In our model (experiments ALT_bio and ALT_satbio) bioturbation is switched fully back on at 65 ka, and the consequential transition in wt % $CaCO_3$ is comparatively gradual. The BFAR record (Figure 5a) suggests a more drawn-out recovery of the benthos and attendant gradual increase in the intensity of bioturbation. If implemented in the model, we would expect a sharper transition at the end of the ETM2 horizon, closer to observations.

If the above analysis is correct and the attributes of the ETM2 horizon at Site 1263 are primarily driven by a local circulation change and its associated benthic ecological impact, this creates a challenge for understanding when these additional effects occurred relative to the primarily CO_2-driven carbonate dissolution at greater depth. In our age model, we adopt the same tie point as *Stap et al*. [2009] to define the start of ETM2 (0 ka in, e.g., Figure 2). This places the required circulation change at Site 1263 approximately coincident with peak ETM2 conditions at 1262. If we shifted the record for 1263 older by one precession cycle instead, the circulation change would occur close to the ETM2 onset at 1262. This would be a plausible alternative alignment, particularly if the carbon release was rapid.

Finally, our failure to explain the full magnitude of observed $\delta^{13}C$ changes at Site 1263 (and not explored here in the model—also of $\delta^{18}O$) is more difficult to account for. We thus do not rule out that differential dissolution or diagenetic alteration might explain some of the observed disparity in bulk carbonate proxy responses between sites. However, the carbon isotope signals in marine carbonate are generally thought

to not be significantly affected by diagenesis [*Sexton et al.*, 2006] and burial depth [*Schrag et al.*, 1995]. Furthermore, differences between the bulk $\delta^{13}C$ values at the two sites are not likely caused by differences in the nannoplankton assemblage composition, because vital effects are minor [*Ziveri et al.*, 2003] and assemblages at the sites similar [*Agnini et al.*, 2007; *Raffi and De Bernardi*, 2008; *Dedert et al.*, 2012]. Although there is some variation in the relative proportions of the CF (foraminifera) and FF (nannoplankton) during the ETM2, the ratio continues to be dominated by calcareous nannofossils (Figure 4d). For $\delta^{18}O$, recrystallization [*Schrag et al.*, 1995] could potentially imprint a component of bottom water temperature at Site 1263, but this would imply that the 1262 record reflects extensive recrystallization because of the lower bottom water temperatures at that site. This seems rather unlikely as burial depths were on the order of 100 m only at Site 1262, i.e., much less than the >300 m at Site 1263, and recrystallization should have been much less pronounced at the deeper site [*Zachos et al.*, 2004a]. None of these diagenetic-based explanations are thus particularly compelling.

5. Conclusions

During the ETM2, Walvis Ridge Sites 1263 and 1262 both record a $\delta^{13}C$ excursion, warming, and evidence of ocean acidification. The benthic foraminiferal ecosystem was perturbed in response to environmental change during the ETM2, with a decrease in abundance, diversity, and assemblage change at both sites. However, a more severe benthic response occurred at the shallow site, resulting in the temporary absence of benthic foraminifers. We infer that this was caused by more pronounced intermediate water warming, leading to effective decline in food supply and deoxygenation driven by a circulation change. This in turn led to a cessation of bioturbation and a possible accentuation of the sedimentological record of the event at 1263. We used a simple conceptual carbon forcing model for a temporary cessation of sediment mixing plus a decrease in carbonate saturation associated with changing intermediate water mass properties. Using this model, we can qualitatively account for the bulk sediment and carbon isotopic observations at both sites. However, a full explanation for the greater magnitude of recorded isotopic excursion at Site 1263 remains to be identified. Our study illustrates that the biotic response to a global change event can be highly spatially heterogeneous and not necessarily scale simply with the magnitude of the event. Instead, the effects of increased atmospheric CO_2 can lead to ocean circulation change and other feedback that create a far more complex picture of the influence of climate change on biota. In turn, changes in biota can distort the sedimentary proxy record.

Acknowledgments
This work was supported by a Royal Society University Research Fellowship awarded each to A. Ridgwell and D. Schmidt and NERC grant NE/H023852/1 (to A. Ridgwell and D. Schmidt). E. Thomas was supported by the Leverhulme Trust and NSF grants OCE-0903014 and OCE-1232413. S. Jennions was supported by a donation through the University of Bristol Alumni Foundation—special thanks to two benefactors who have made this research possible. Data are available at Pangaea, http://doi.pangaea.de/10.1594/PANGAEA.845418.

References

Abels, H. A., W. C. Clyde, P. D. Gingerich, F. J. Hilgen, H. C. Fricke, G. J. Bowen, and L. J. Lourens (2012), Terrestrial carbon isotope excursions and biotic change during Palaeogene hyperthermals, *Nat. Geosci.*, *5*(5), 326–329.

Agnini, C., E. Fornaciari, D. Rio, F. Tateo, J. Backman, and L. Giusberti (2007), Responses of calcareous nannofossil assemblages, mineralogy and geochemistry to the environmental perturbations across the Paleocene/Eocene boundary in the Venetian Pre-Alps, *Mar. Micropaleontol.*, *63*(1), 19–38.

Agnini, C., P. Macrì, J. Backman, H. Brinkhuis, E. Fornaciari, L. Giusberti, V. Luciani, D. Rio, A. Sluijs, and F. Speranza (2009), An early Eocene carbon cycle perturbation at ~52.5 Ma in the southern Alps: Chronology and biotic response, *Paleoceanography*, *24*, PA2209, doi:10.1029/2008PA001.

Alegret, L., S. Ortiz, I. Arenillas, and E. Molina (2010), What happens when the ocean is overheated? The foraminiferal response across the Paleocene-Eocene Thermal Maximum at the Alamedilla section (Spain), *Geol. Soc. Am. Bull.*, *122*(9–10), 1616–1624.

Archer, D., et al. (2009), Atmospheric lifetime of fossil fuel carbon dioxide, *Annu. Rev. Earth Planet. Sci.*, *37*(1), 117.

Bopp, L., et al. (2013), Multiple stressors of ocean ecosystems in the 21st century: Projections with CMIP5 models, *Biogeosciences*, *10*, 6225–6245.

Bralower, T. J. (2002), Evidence of surface water oligotrophy during the Paleocene-Eocene Thermal Maximum: Nannofossil assemblage data from Ocean Drilling Program Site 690, Maud Rise, Weddell Sea, *Paleoceanography*, *17*(2), 1023, doi:10.1029/2001PA000662.

Bremer, M., and G. Lohmann (1982), Evidence for primary control of the distribution of certain Atlantic Ocean benthonic foraminifera by degree of carbonate saturation, *Deep Sea Res., Part A*, *29*(8), 987–998.

Caldeira, K., and M. E. Wickett (2003), Oceanography: Anthropogenic carbon and ocean pH, *Nature*, *425*(6956), 365–365.

Chun, C. O. J., M. L. Delaney, and J. C. Zachos (2010), Paleo-redox changes across the Paleocene-Eocene Thermal Maximum, Walvis Ridge (ODP Sites 1262, 1263, and 1266): Evidence from Mn and U enrichment factors, *Paleoceanography*, *25*, PA4202, doi:10.1029/2009PA0018.

Clementz, M., S. Bajpai, V. Ravikant, J. G. M. Thewissen, N. Saravanan, I. B. Singh, and V. Prasad (2011), Early Eocene warming events and the timing of terrestrial faunal exchange between India and Asia, *Geology*, *39*(1), 15–18.

Colbourn, G., A. Ridgwell, and T. M. Lenton (2013), The Rock Geochemical Model (RokGeM) v0.9, *Geosci. Model Dev.*, *6*(5), 1543–1573.

Coma, R., M. Ribes, E. Serrano, E. Jiménez, J. Salat, and J. Pascual (2009), Global warming-enhanced stratification and mass mortality events in the Mediterranean, *Proc. Natl. Acad. Sci. U.S.A.*, *106*(15), 6176–6181.

Cramer, B. S., J. D. Wright, D. V. Kent, and M. P. Aubry (2003), Orbital climate forcing of $\delta^{13}C$ excursions in the late Paleocene–early Eocene (chrons C24n–C25n), *Paleoceanography*, *18*(4), 1097, doi:10.1029/2003PA000909.

Crouch, E. M., C. Heilmann-Clausen, H. Brinkhuis, H. E. Morgans, K. M. Rogers, H. Egger, and B. Schmitz (2001), Global dinoflagellate event associated with the late Paleocene Thermal Maximum, *Geology*, *29*(4), 315–318.

Dedert, M., H. M. Stoll, D. Kroon, N. Shimizu, K. Kanamaru, and P. Ziveri (2012), Productivity response of calcareous nannoplankton to Eocene Thermal Maximum 2 (ETM2), *Clim. Past*, *8*(3), 977–993.
d'Haenens, S., A. Bornemann, P. Stassen, and R. P. Speijer (2012), Multiple early Eocene benthic foraminiferal assemblage and $\delta^{13}C$ fluctuations at DSDP Site 401 (Bay of Biscay—NE Atlantic), *Mar. Micropaleontol.*, *88*, 15–35.
d'Haenens, S., A. Bornemann, P. Claeys, U. Röhl, E. Steurbaut, and R. P. Speijer (2014), A transient deep-sea circulation switch during Eocene Thermal Maximum 2 (ETM2), *Paleoceanography*, *29*, 370–388, doi:10.1002/2013PA002567.
Dickens, G. R., M. M. Castillo, and J. C. Walker (1997), A blast of gas in the latest Paleocene: Simulating first-order effects of massive dissociation of oceanic methane hydrate, *Geology*, *25*(3), 259–62.
Dunkley Jones, T., D. J. Lunt, D. N. Schmidt, A. Ridgwell, A. Sluijs, P. J. Valdes, and M. Maslin (2013), Climate model and proxy data constraints on ocean warming across the Paleocene–Eocene Thermal Maximum, *Earth Sci. Rev.*, *125*, 123–145.
Durack, P. J., S. E. Wijffels, and R. J. Matear (2012), Ocean salinities reveal strong global water cycle intensification during 1950 to 2000, *Science*, *336*(6080), 455–458.
Foster, L. C., D. N. Schmidt, E. Thomas, S. Arndt, and A. Ridgwell (2013), Surviving rapid climate change in the deep sea during the Paleogene hyperthermals, *Proc. Natl. Acad. Sci. U.S.A.*, *110*(23), 1–4.
Gibbs, S. J., T. J. Bralower, P. R. Bown, J. C. Zachos, and L. M. Bybell (2006), Shelf and open-ocean calcareous phytoplankton assemblages across the Paleocene-Eocene Thermal Maximum: Implications for global productivity gradients, *Geology*, *34*(4), 233.
Gooday, A. (2003), Benthic foraminifera (Protista) as tools in deep-water palaeoceanography: Environmental influences on faunal characteristics, *Adv. Mar. Biol.*, *46*, 1–90.
Gooday, A. J., and F. J. Jorissen (2012), Benthic foraminiferal biogeography: Controls on global distribution patterns in deep-water settings, *Annu. Rev. Mar. Sci.*, *4*(1), 237–262.
Gooday, A. J., B. J. Bett, E. Escobar, B. Ingole, L. A. Levin, C. Neira, A. V. Raman, and J. Sellanes (2010), Habitat heterogeneity and its influence on benthic biodiversity in oxygen minimum zones, *Mar. Ecol.*, *31*(1), 125–147.
Grosse, O. (2002), Sediment interactions of foraminifera: Implications for food degredation and bioturbation processes, *J. Foraminiferal Res.*, *32*(4), 414–424.
Hayward, B. W., S. Kawagata, A. T. Sabaa, H. R. Grenfell, L. van Kerckhoven, K. Johnson, and E. Thomas (2012), *The Last Global Extinction (Mid-Pleistocene) of Deep-Sea Benthic Foraminifera (Chrysalogoniidae, Ellipsoidinidae, Glandulonodosariidae, Plectofrondicularidae, Pleurostomellidae, Stilostomellidae), Their Late Cretaceous-Cenozoic History and Taxonomy*, *Spec. Publ.*, vol. 43, 408 pp., Cushman Foundation Foraminiferal Reseach, Cambridge, U. K.
Herguera, J., and W. Berger (1991), Paleoproductivity from benthic foraminifera abundance: Glacial to postglacial change in the west-equatorial Pacific, *Geology*, *19*(12), 1173–1176.
Hochachka, P. W., and G. N. Somero (2002), *Biochemical Adaptation: Mechanism and Process in Physiological Evolution*, 480th ed., Oxford Univ. Press, New York.
Hoegh-Guldberg, O., and J. F. Bruno (2010), The impact of climate change on the world's marine ecosystems, *Science*, *328*(5985), 1523–8.
Hollis, C. J. (2006), Radiolarian faunal turnover through the Paleocene-Eocene transition, Mead Stream, New Zealand, in *Radiolaria*, pp. 79–99, Birkhäuser, Basel, Switzerland.
Hönisch, B., et al. (2012), The geological record of ocean acidification, *Science*, *335*(6072), 1058–1063.
Hutchins, D. A., F.-X. Fu, Y. Zhang, M. E. Warner, Y. Feng, K. Portune, P. W. Bernhardt, and M. R. Mulholland (2007), CO_2 control of Trichodesmium N_2 fixation, photosynthesis, growth rates, and elemental ratios: Implications for past, present, and future ocean biogeochemistry, *Limnol. Oceanogr.*, *52*(4), 1293–1304.
John, E. H., J. D. Wilson, P. N. Pearson, and A. Ridgwell (2014), Temperature-dependent remineralization and carbon cycling in the warm Eocene oceans, *Palaeogeogr. Palaeoclimatol. Palaeoecol.*, *413*, 158–166.
Jorissen, F. J., H. C. de Stigter, and J. G. V. Widmark (1995), A conceptual model explaining benthic foraminiferal microhabitats, *Mar. Micropaleontol.*, *26*(1–4), 3–15.
Jorissen, F., C. Fontanier, and E. Thomas (2007), Paleoceanographical proxies based on deep-sea benthic foraminiferal assemblage characteristics, in *Proxies in Late Cenozoic Paleoceanography: Pt. 2: Biological Tracers and Biomarkers*, edited by C. Hillaire-Marcel and A. de Vernal, pp. 263–326, Elsevier, Oxford, U. K.
Keeling, R. F., A. Körtzinger, and N. Gruber (2010), Ocean deoxygenation in a warming world, *Annu. Rev. Mar. Sci.*, *2*(1), 199–229.
Kelly, D. C., T. J. Bralower, J. C. Zachos, I. P. Silva, and U. Milano (1996), Rapid diversification of planktonic foraminifera in the tropical Pacific (ODP Site 865) during the late Paleocene Thermal Maximum, *Geology*, *24*, 423–426.
Kelly, D. C., J. C. Zachos, T. J. Bralower, and S. A. Schellenberg (2005), Enhanced terrestrial weathering/runoff and surface ocean carbonate production during the recovery stages of the Paleocene-Eocene Thermal Maximum, *Paleoceanography*, *20*, PA4023, doi:10.1029/2005PA001163.
Kirtland Turner, S., and A. Ridgwell (2013), Recovering the true size of an Eocene hyperthermal from the marine sedimentary record, *Paleoceanography*, *28*, 700–712, doi:10.1002/2013PA002541.
Kroeker, K. J., R. L. Kordas, R. N. Crim, and G. G. Singh (2010), Meta-analysis reveals negative yet variable effects of ocean acidification on marine organisms, *Ecol. Lett.*, *13*(11), 1419–1434.
Kump, L., T. Bralower, and A. Ridgwell (2009), Ocean acidification in deep time, *Oceanography*, *22*(4), 94–107.
Le, J., and N. Shackleton (1992), Carbonate dissolution fluctuations in the western equatorial Pacific during the late Quaternary, *Paleoceanography*, *7*(1), 21–42, doi:10.1029/91PA02854.
Linke, P. (1992), Metabolic adaptations of deep-sea benthic foraminifera to seasonally varying food input, *Mar. Ecol. Prog. Ser. Oldendorf*, *81*, 51–63.
Littler, K., U. Röhl, T. Westerhold, and J. C. Zachos (2014), A high-resolution benthic stable-isotope record for the South Atlantic: Implications for orbital-scale changes in late Paleocene-early Eocene climate and carbon cycling, *Earth Planet. Sci. Lett.*, *401*, 18–30.
Lourens, L. J., A. Sluijs, D. Kroon, J. C. Zachos, E. Thomas, U. Röhl, J. Bowles, and I. Raffi (2005), Astronomical pacing of late Palaeocene to early Eocene global warming events, *Nature*, *435*(7045), 1083–7.
Luciani, V., L. Giusberti, C. Agnini, J. Backman, E. Fornaciari, and D. Rio (2007), The Paleocene–Eocene Thermal Maximum as recorded by Tethyan planktonic foraminifera in the Forada section (northern Italy), *Mar. Micropaleontol.*, *64*(3–4), 189–214.
Lunt, D. J., P. J. Valdes, T. D. Jones, A. Ridgwell, A. M. Haywood, D. N. Schmidt, R. Marsh, and M. Maslin (2010), CO_2-driven ocean circulation changes as an amplifier of Paleocene-Eocene Thermal Maximum hydrate destabilization, *Geology*, *38*(10), 875–878.
Ma, Z., E. Gray, E. Thomas, and B. Murphy (2014), Carbon sequestration during the Palaeocene-Eocene Thermal Maximum by an efficient biological pump, *Nat. Geosci.*, *7*, 382–388.

Mahowald, N., M. Yoshioka, W. Collins, A. Conley, D. Fillmore, and D. Coleman (2006), Climate response and radiative forcing from mineral aerosols during the glacial maximum, pre-industrial, current and doubled-carbon dioxide climates, *Geophys. Res. Lett.*, *33*, L20705, doi:10.1029/2006GL026126.

Mancin, N., B. W. Hayward, I. Trattenero, M. Cobianchi, and C. Lupi (2013), Can the morphology of deep-sea benthic foraminifera reveal what caused their extinction during the mid-Pleistocene Climate Transition?, *Mar. Micropaleontol.*, *104*, 53–70.

McCarren, H., E. Thomas, T. Hasegawa, U. Röhl, and J. C. Zachos (2008), Depth dependency of the Paleocene-Eocene carbon isotope excursion: Paired benthic and terrestrial biomarker records (Ocean Drilling Program Leg 208, Walvis Ridge), *Geochem. Geophys. Geosyst.*, *9*, Q10008, doi:10.1029/2008GC002116.

Melzner, F., J. Thomsen, W. Koeve, A. Oschlies, M. A. Gutowska, H. W. Bange, H. P. Hansen, and A. Körtzinger (2013), Future ocean acidification will be amplified by hypoxia in coastal habitats, *Mar. Biol.*, *160*(8), 1875–1888.

Nguyen, T. M. P., and R. P. Speijer (2014), A new procedure to assess dissolution based on experiments on Pliocene–Quaternary foraminifera (ODP Leg 160, Eratosthenes Seamount, Eastern Mediterranean), *Mar. Micropaleontol.*, *106*, 22–39.

Nguyen, T. M. P., M. P. Petrizzo, and R. Speijer (2009), Experimental dissolution of a fossil foraminiferal assemblage (Paleocene-Eocene Thermal Maximum, Dababiya, Egypt): Implications for paleoenvironmental reconstructions, *Mar. Micropaleontol.*, *73*(3), 241–258.

Nicolo, M. J., G. R. Dickens, C. J. Hollis, and J. C. Zachos (2007), Multiple early Eocene hyperthermals: Their sedimentary expression on the New Zealand continental margin and in the deep sea, *Geology*, *35*(8), 699–702.

Nicolo, M. J., G. R. Dickens, and C. J. Hollis (2010), South Pacific intermediate water oxygen depletion at the onset of the Paleocene-Eocene Thermal Maximum as depicted in New Zealand margin sections, *Paleoceanography*, *25*, PA4210, doi:10.1029/2009PA001904.

Norris, R. D., S. K. Turner, P. M. Hull, and A. Ridgwell (2013), Marine ecosystem responses to Cenozoic global change, *Science*, *341*(6145), 492–8.

O'Connor, M. I., M. F. Piehler, D. M. Leech, A. Anton, and J. F. Bruno (2009), Warming and resource availability shift food Web structure and metabolism, *PLoS Biol.*, *7*(8), e1000178, doi:10.1371/journal.pbio.1000178.

Pälike, C., M. Delaney, and J. Zachos (2014), Deep-sea redox across the Paleocene-Eocene Thermal Maximum, *Geochem. Geophys. Geosyst.*, *15*, 1038–1053, doi:10.1002/2013GC005074.

Panchuk, K., A. Ridgwell, and L. R. Kump (2008), Sedimentary response to Paleocene-Eocene Thermal Maximum carbon release: A model-data comparison, *Geology*, *36*(4), 315–318.

Penman, D. E., B. Hönisch, R. E. Zeebe, E. Thomas, and J. C. Zachos (2014), Rapid and sustained surface ocean acidification during the Paleocene-Eocene Thermal Maximum, *Paleoceanography*, *29*, 357–369, doi:10.1002/2014PA002621.

Pörtner, H.-O., D. Karl, P. W. Boyd, W. Cheung, S. E. Lluch-Cota, Y. Nojiri, D. Schmidt, and P. Zavialov (2014), Ocean systems, in *Climate Change 2014: IPCC WGII AR5*, pp. 411–484, Cambridge Univ. Press, Cambridge, U. K., and New York.

Post, J. E., E. Thomas, and P. J. Heaney (2015), Jianshuiite in oceanic manganese nodules, *Am. Mineral.*, in revision.

Raffi, I., and B. De Bernardi (2008), Response of calcareous nannofossils to the Paleocene–Eocene Thermal Maximum: Observations on composition, preservation and calcification in sediments from ODP Site 1263 (Walvis Ridge—SW Atlantic), *Mar. Micropaleontol.*, *69*(2), 119–138.

Raffi, I., J. Backman, E. Fornaciari, H. Pälike, D. Rio, L. Lourens, and F. Hilgen (2006), A review of calcareous nannofossil astrobiochronology encompassing the past 25 million years, *Quat. Sci. Rev.*, *25*(23), 3113–3137.

Ravizza, G., R. N. Norris, J. Blusztajn, and M. P. Aubry (2001), An osmium isotope excursion associated with the late Paleocene Thermal Maximum: Evidence of intensified chemical weathering, *Paleoceanography*, *16*(2), 155–163, doi:10.1029/2000PA000541.

Ridgwell, A. (2007), Application of sediment core modelling to interpreting the glacial-interglacial record of Southern Ocean silica cycling, *Clim. Past*, *3*, 387–396.

Ridgwell, A., and D. N. Schmidt (2010), Past constraints on the vulnerability of marine calcifiers to massive carbon dioxide release, *Nat. Geosci.*, *3*(3), 196–200.

Ridgwell, A. J. (2001), Glacial-interglacial perturbations in the global carbon cycle, Doctoral dissertation, Univ. of East Anglia.

Schneider, L. J., T. J. Bralower, L. R. Kump, and M. E. Patzkowsky (2013), Calcareous nannoplankton ecology and community change across the Paleocene-Eocene Thermal Maximum, *Paleobiology*, *39*(4), 628–647.

Schrag, D., D. DePaolo, and F. Richter (1995), Reconstructing past sea surface temperatures: Correcting for diagenesis of bulk marine carbonate, *Geochim. Cosmochim. Acta*, *59*(11), 2265–2278.

Sexton, P. F., P. A. Wilson, and P. N. Pearson (2006), Microstructural and geochemical perspectives on planktic foraminiferal preservation: "Glassy" versus "frosty", *Geochem. Geophys. Geosyst.*, *7*, Q12P19, doi:10.1029/2006GC001291.

Slotnick, B. S., G. R. Dickens, M. J. Nicolo, C. J. Hollis, J. S. Crampton, J. C. Zachos, and A. Sluijs (2012), Large-amplitude variations in carbon cycling and terrestrial weathering during the latest Paleocene and earliest Eocene: The record at Mead Stream, New Zealand, *J. Geol.*, *120*(5), 487–505.

Sluijs, A., et al. (2006), Subtropical Arctic Ocean temperatures during the Palaeocene/Eocene Thermal Maximum, *Nature*, *441*(7093), 610–613.

Sluijs, A., H. Brinkhuis, S. Schouten, S. M. Bohaty, C. M. John, J. C. Zachos, G.-J. Reichart, J. S. S. Damsté, E. M. Crouch, and G. R. Dickens (2007a), Environmental precursors to rapid light carbon injection at the Palaeocene/Eocene boundary, *Nature*, *450*(7173), 1218–1221.

Sluijs, A., G. J. Bowen, H. Brinkhuis, L. J. Lourens, and E. Thomas (2007b), The Palaeocene–Eocene Thermal Maximum super greenhouse: Biotic and geochemical signatures, age models and mechanisms of global change, in *Deep Time Perspectives on Climate Change: Marrying the Signal From Computer Models and Biological Proxies*, edited by M. Williams et al., pp. 323–347, Geol. Soc., London.

Sluijs, A., S. Schouten, T. H. Donders, P. L. Schoon, U. Röhl, G.-J. Reichart, F. Sangiorgi, J.-H. Kim, J. S. Sinninghe Damsté, and H. Brinkhuis (2009), Warm and wet conditions in the Arctic region during Eocene Thermal Maximum 2, *Nat. Geosci.*, *2*(11), 777–780.

Sluijs, A., L. Van Roij, G. J. Harrington, S. Schouten, J. A. Sessa, L. J. Levay, G. J. Reichart, and C. P. Slomp (2014), Warming, euxinia and sea level rise during the Paleocene-Eocene Thermal Maximum on the Gulf Coastal Plain: Implications for ocean oxygenation and nutrient cycling, *Clim. Past*, *10*(4), 1421–1439.

Solomon, S., G.-K. Plattner, R. Knutti, and P. Friedlingstein (2009), Irreversible climate change due to carbon dioxide emissions, *Proc. Natl. Acad. Sci. U.S.A.*, *106*(6), 1704–1709.

Speijer, R., C. Scheibner, P. Stassen, and A. M. M. Morsi (2012), Response of marine ecosystems to deep-time global warming: A synthesis of biotic patterns across the Paleocene-Eocene Thermal Maximum (PETM), *Aust. J. Earth Sci.*, *105*(1), 6–16.

Stap, L., A. Sluijs, E. Thomas, and L. Lourens (2009), Patterns and magnitude of deep sea carbonate dissolution during Eocene Thermal Maximum 2 and H2, Walvis Ridge, southeastern Atlantic Ocean, *Paleoceanography*, *24*, PA1211, doi:10.1029/2008PA001655.

Stap, L., L. Lourens, A. van Dijk, S. Schouten, and E. Thomas (2010a), Coherent pattern and timing of the carbon isotope excursion and warming during Eocene Thermal Maximum 2 as recorded in planktic and benthic foraminifera, *Geochem. Geophys. Geosyst.*, *11*, Q11011, doi:10.1029/2010GC003097.

Stap, L., L. J. Lourens, E. Thomas, A. Sluijs, S. Bohaty, and J. C. Zachos (2010b), High-resolution deep-sea carbon and oxygen isotope records of Eocene Thermal Maximum 2 and H2, *Geology*, *38*(7), 607–610.

Stassen, P., E. Thomas, and R. Speijer (2015), Paleocene-Eocene Thermal Maximum environmental change in the New Jersey Coastal Plain: Benthic foraminiferal biotic events, *Mar. Micropaleontol.*, *115*, 1–23.

Stein, R., B. Boucsein, and H. Meyer (2006), Anoxia and high primary production in the Paleogene central Arctic Ocean: First detailed records from Lomonosov Ridge, *Geophys. Res. Lett.*, *33*, L18606, doi:10.1029/2006GL026776.

Steineck, P., and E. Thomas (1996), The latest Paleocene crisis in the deep sea: Ostracode succession at Maud Rise, Southern Ocean, *Geology*, *7*, 583–586.

Thomas, E. (1998), Biogeography of the late Paleocene benthic foraminiferal extinction, in *Late Paleocene-Early Eocene Climatic and Biotic Events in the Marine and Terrestrial Records*, edited by M. P. Aubry, S. Lucas, and W. A. Berggren, pp. 214–243, Columbia Univ. Press, New York.

Thomas, E. (2003), Extinction and food at the seafloor: A high-resolution benthic foraminiferal record across the Initial Eocene Thermal Maximum, Southern Ocean Site 690, Abstract 80301(303).

Thomas, E. (2007), Cenozoic mass extinctions in the deep sea: What perturbs the largest habitat on Earth?, *Geol. Soc. Am. Spec. Pap.*, *424*(01), 1–23.

Thomas, E., and A. Gooday (1996), Cenozoic deep-sea benthic foraminifers: Tracers for changes in oceanic productivity?, *Geology*, *24*(4), 355–358.

Thomas, E., and N. J. Shackleton (1996), The Paleocene-Eocene benthic foraminiferal extinction and stable isotope anomalies, *Geol. Soc. London Spec. Publ.*, *101*(1), 401–441.

Thomas, E., and J. C. Zachos (2000), Was the late Paleocene Thermal Maximum a unique event?, *GFF*, *122*(1), 169–170.

Tindall, J., R. Flecker, P. Valdes, D. N. Schmidt, P. Markwick, and J. Harris (2010), Modelling the oxygen isotope distribution of ancient seawater using a coupled ocean–atmosphere GCM: Implications for reconstructing early Eocene climate, *Earth Planet. Sci. Lett.*, *292*(3–4), 265–273.

Westerhold, T., U. Röhl, J. Laskar, I. Raffi, J. Bowles, L. J. Lourens, and J. C. Zachos (2007), On the duration of magnetochrons C24r and C25n and the timing of early Eocene global warming events: Implications from the Ocean Drilling Program Leg 208 Walvis Ridge depth transect, *Paleoceanography*, *22*, PA2201, doi:10.1029/2006PA001322.

Westerhold, T., U. Röhl, and J. Laskar (2012), Time scale controversy: Accurate orbital calibration of the early Paleogene, *Geochem. Geophys. Geosyst.*, *13*, Q06015, doi:10.1029/2012GC004096.

Winguth, A. M. E., E. Thomas, and C. Winguth (2012), Global decline in ocean ventilation, oxygenation, and productivity during the Paleocene-Eocene Thermal Maximum: Implications for the benthic extinction, *Geology*, *40*(3), 263–266.

Zachos, J. C., D. Kroon, P. Blum, and Scientific Shipboard Party (2004a), Leg 208, Site 1262 Initial Report, in *Proceedings of the Ocean Drilling Program, Initial Rep.*, vol. 208, pp. 1–112, Ocean Drill. Program, College Station, Tex.

Zachos, J. C., D. Kroon, P. Blum, and Scientific Shipboard Party (2004b), Leg 208, Site1263 Initial Report, in *Proceedings of the Ocean Drilling Program, Initial Rep.*, vol. 208, pp. 77,845–9547, Texas A&M Univ., College Station, Tex.

Zachos, J. C. J., et al. (2005), Rapid acidification of the ocean during the Paleocene-Eocene Thermal Maximum, *Science*, *308*(5728), 1611–1615.

Zhou, X., E. Thomas, R. E. M. Rickaby, A. M. E. Winguth, and Z. Lu (2014), I/Ca evidence for upper ocean deoxygenation during the PETM, *Paleoceanography*, *29*, 964–975, doi:10.1002/2014PA002702.

Ziveri, P., H. Stoll, I. Probert, C. Klaas, M. Geisen, G. Ganssen, and J. Young (2003), Stable isotope "vital effects" in coccolith calcite, *Earth Planet. Sci. Lett.*, *210*(1–2), 137–149.